Coronography with adaptive optics: the ADONIS coronograph

Jean-Luc Beuzit[1], David Mouillet[2], Anne-Marie Lagrange[2], David Le Mignant[3]

[1] Canada-France-Hawaii Telescope, 65-1238 Mamalahoa Highway, Kamuela, HI 96743, U.S.A.
[2] Laboratoire d'Astrophysique, Observatoire de Grenoble, B.P. 53, 38041 Grenoble Cedex, France
[3] ESO Santiago, Casilla 19001, Santiago 19, Chile

Abstract

The combination of adaptive optics and coronographic techniques providing at the same time high angular resolution and high dynamic range is a powerful tool to study the close environment of bright objects in different fields of astrophysics (search for brown dwarfs and giant extra-solar planets around nearby stars, search for circumstellar disks, study of AGB outflows, etc). We present in this paper the design and performance analysis of the ADONIS coronograph, discuss the observing and data reduction strategy, and illustrate its application to a few astrophysical programmes.

1 Introduction

By using an occulting mask to block the flux of a bright object, coronographic techniques allow to explore its close environment to search for faint sources like stellar or sub-stellar companions, disks or envelopes. For instance, in 1984, a circumstellar disk has been detected around the star β Pictoris (Smith & Terrile 1984) using a coronograph with a $7''$ diameter occulting mask. More recently, an infrared coronograph has been designed to search for brown dwarfs around nearby red dwarfs at CFHT (Beuzit et al. 1990). Clampin et al. (1994) have also built a coronograph optimized for the excellent image quality obtained with the ESO NTT at La Silla. The main limiting factor for all these coronographs was the lack of spatial resolution. An obvious way to avoid atmospheric turbulence is to observe from space. For example, the NICMOS coronograph on HST allows the direct detection of low mass companions with a dynamic range of $\Delta\, m_H \sim 12$ down to $1''$ from the central star (Lowrance et al. 1998). For ground-based observations, the coupling with adaptive optics greatly improves the efficiency of coronographic imaging: the adaptive optics system concentrates the flux from the bright source and reduces the wings of the point spread function (PSF), therefore allowing the use of smaller occulting masks and consequently the exploration of a closest region around the central object. The improvement with the use of partial image correction has already been demonstrated on the COME-ON adaptive optics system (Malbet 1996) and by the Adaptive Optics Coronagraph (Golimowski, Durrance, & Clampin 1993). On the basis of the COME-ON experiment, we have built a coronograph (Beuzit et al. 1997b) to work with the ADONIS adaptive optics system on the ESO 3.6 meter telescope at La Silla, which provides diffraction-limited images in K band (2.2 μm), i.e. a resolution of $0.12''$ (Beuzit et al. 1997a). This coronograph has been used from 1994 to 1997 as a visitor instrument by a team from Observatoire de Grenoble (Mouillet et al. 1997a). Based on this experience, a new coronograph has recently been designed and manufactured, under contract with ESO, to be used as a pre-focal optics of the SHARP infrared camera on the ADONIS adaptive optics system. This new coronographic mode has been offered to the ESO community in March 1998.

The paper is organized as follows. In section 2 we present the design of the new coronograph, in section 3 we assess its performance and in section 4 we discuss the observation and data reduction strategy. The use of the coronograph in the context of a few astrophysical programmes is illustrated in section 5 and finally the potential benefit of applying coronographic techniques to very large telescopes is reviewed in section 6.

2 The ADONIS coronograph

The optical sketch of the new ADONIS coronograph is illustrated by Fig. 1. This coronograph consists of two parts, the focal plane unit located at the F/45 output focus of the ADONIS adaptive optics system and the cold Lyot stop, inside the SHARP infrared camera, which is optically conjugated with the telescope pupil.

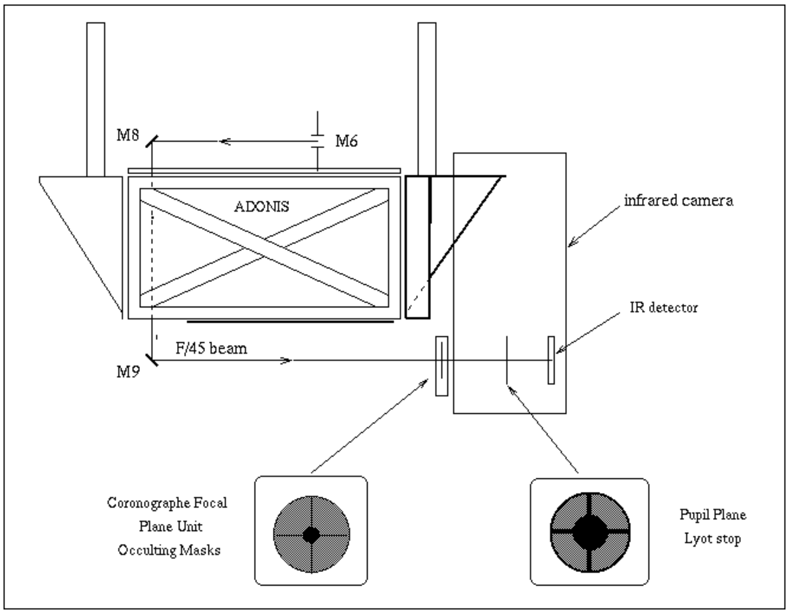

Figure 1: Optical sketch of the ADONIS coronograph.

2.1 Focal plane unit

The coronograph focal plane unit (Fig. 2) is directly fixed to the infrared camera support. Its function is to permit the insertion of the occulting masks at the ADONIS F/45 output focal plane. Several occulting masks are available, with diameters ranging from 0.4″ to 5.5″ on the sky. The masks are mounted on dedicated barrels, each of them supporting up to 3 masks (Fig. 2 and Table 1). Any of these three masks can be remotely inserted in the camera field of view in a matter of seconds. The control of the mask selection and positioning is part of the infrared camera acquisition software.

The occulting masks that are presently being used on the ADONIS coronograph consist of laser machined aluminium foils, suspended by means of thin (10 μm in diameter) tungsten wires, on which they are glued. They have been manufactured using the CFHT LAMA machine (Seerveld 1998). This technique avoids the use of any optical component in the beam, thereby eliminating ghosts as well as chromatic and scattering effects, but does not allow to obtain occulting masks with different transmission functions such as Gaussian ones, etc. Simulations suggest that such masks can improve the rejection performance of coronographs (Watson et al. 1991). We are planning to test occulting masks made of gold coated, infrared transparent substrates with various transmission profiles. If significant improvements are demonstrated, these masks will be made available to observers.

Table 1: Occulting mask diameters on the sky (”).

Barrel 1	0.42	0.63	0.72
Barrel 2	0.84	1.00	1.40
Barrel 3	2.00	3.92	5.50

2.2 Lyot stop

The Lyot stop (Fig. 1) consists of a scaled and slightly undersized copy of the telescope pupil image, including the secondary mirror and the secondary mirror spider, located on a pupil image inside the infrared camera. The external and internal diameters have been respectively reduced and increased by 3% with respect to the actual pupil image, leading to a overall loss of 9% in term of flux.

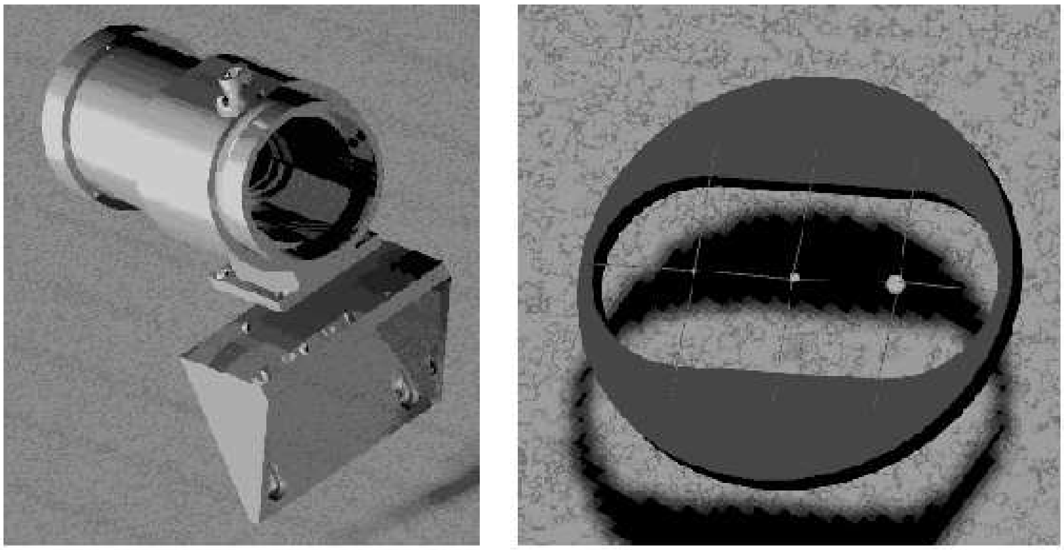

Figure 2: Details of the coronograph focal plane unit and occulting masks.

This cold Lyot stop has two functions:

- limit the instrumental background seen by the detector and generated by the telescope and the ADONIS instrument. This is of course particularly important above 2 μm.
- reduce the amount of scattered light due to the coronograph occulting mask. The bright source energy is uniformly distributed in the entrance pupil plane (telescope primary mirror). In the pupil plane located after the focal occulting mask, the residual energy from this centered source is concentrated at the border of the pupil image (Figs. 3 and 4). The larger the occulting mask, the more concentrated is the residual light. By reducing the effective pupil size, the Lyot mask allows the rejection of this residual light. Simulations have shown that a reduction of 3% of the pupil image diameter was well suited for this apodization effect.

3 Performance

The ADONIS coronograph has been tested in January 1998 both in the laboratory using the ADONIS artificial source and at the telescope. These tests demonstrate an excellent behaviour of the coronograph: very regular shape of the occulting masks, no reflection pattern from any part of the coronograph focal plane unit is detected, the wires supporting the occulting masks induce a very low signature on the detector (2 pixels wide and a few ADUs in level), the accuracy on the positioning of the occulting masks is better than $0.003''$ ie. 1/10 pixel for the smallest pixel scale of the SHARP camera.

The performance in terms of detectivity is illustrated in Fig. 5 for two different diameters of the occulting mask, respectively $0.8''$ and $1.4''$. These results have been obtained in the H band (1.65 μm) for a total integration time of 300 seconds on a star of $m_H = 6$. The upper curve shows the profile of the star outside of the mask. The second curve shows the profile of the occulted star scaled to the same exposure time as the unocculted one. The lower curve corresponds to the one sigma detection limit per pixel after subtraction of the PSF wings measured on a comparison star observed in the same conditions. This illustrates the cumulative effects of the photon noise and the high order turbulence modes. The flux is expressed in magnitude difference relatively to the brightest pixel of the unocculted star. Fig. 5 shows that the detection limit at $2.5''$, with the $1.4''$ mask, is 10^5 fainter (12.5 magnitude *per pixel*) than the peak intensity of the star observed without the mask, with the same angular resolution.

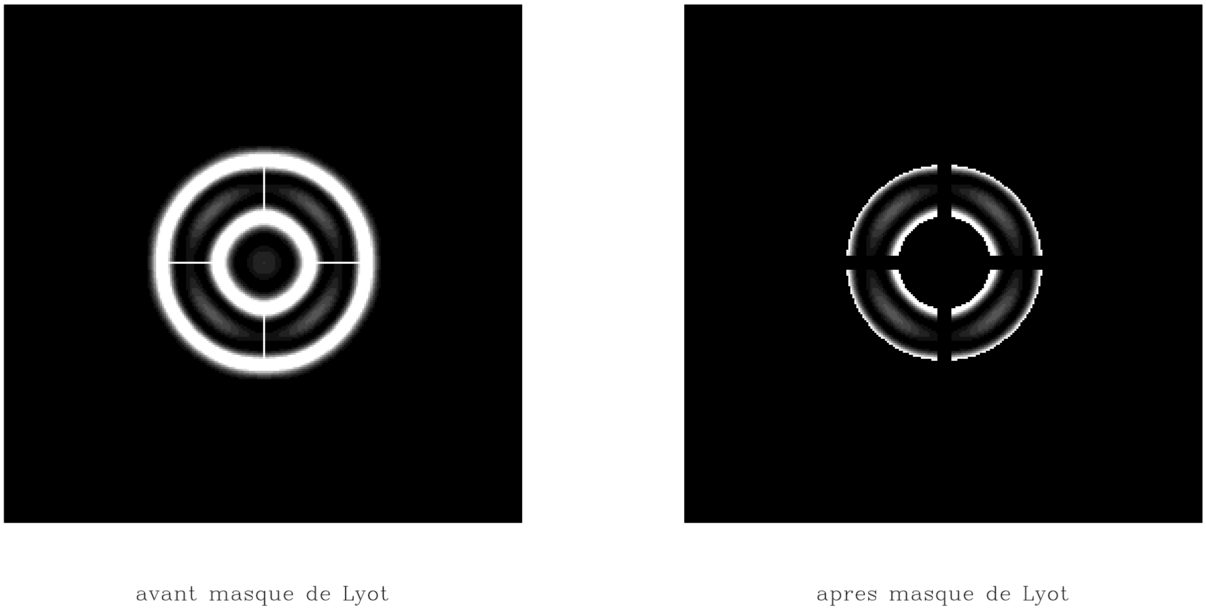

Figure 3: Theoretical computation of the residual energy distribution of an on-axis point-like source over a pupil plane after a $0.8''$ diameter focal occulting mask. Left (resp. right) column shows an image of the pupil before (resp. after) the Lyot mask.

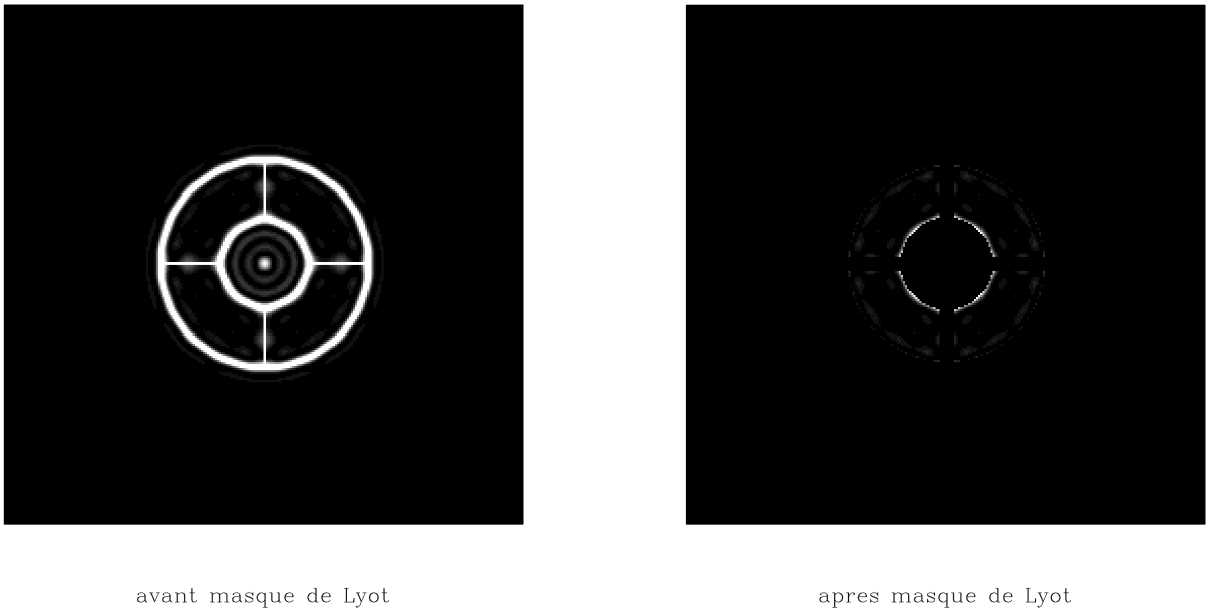

Figure 4: Same as Fig. 3 in the case of a $2''$ diameter occulting mask.

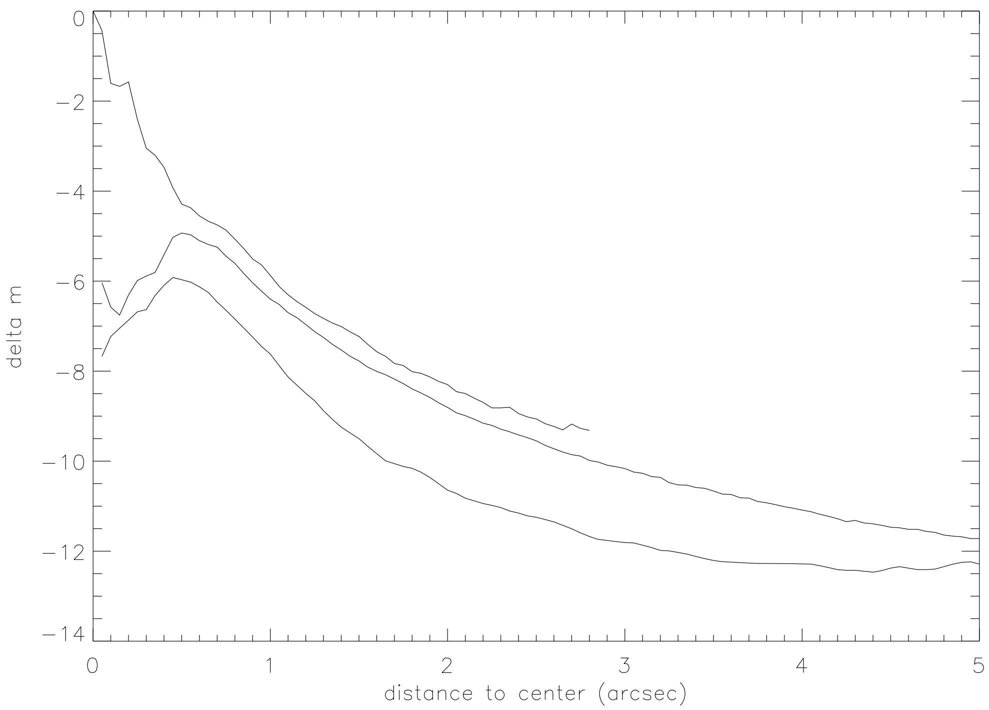

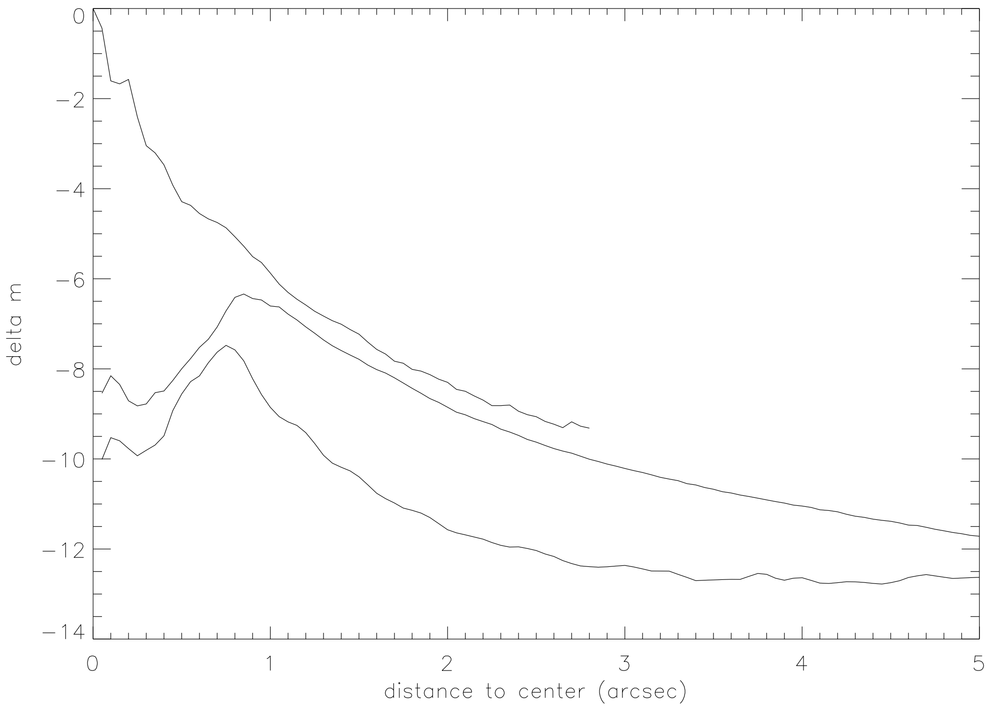

Figure 5: Detectivity of the ADONIS coronograph in H band with 0.8″ (up) and 1.4″ (down) diameter occulting masks.

4 Observations and data reduction

4.1 Observations

A typical observing procedure for a given target consists in recording images of that target with the occulting mask, as well as images obtained without the mask to measure the PSF. Similar observations of a comparison star, obtained under the same conditions of adaptive optics correction, are needed by the reduction procedure, as described in section 4.2. Usually two comparison stars are observed for cross confirmation purposes. For each object, the sky emission is also measured, with the same total integration time, at an angular distance of typically $30''$. Individual exposure times are constrained by the dynamic range of the detector and, on bright targets (m_K = 3–6), are typically of a few seconds. Data cubes of typically 100 images are recorded. In addition, flat-field and dark exposures are taken at the beginning or at the end of the night. Photometric and astrometric calibration stars are also observed.

4.2 Data reduction

The data are first reduced following standard image processing techniques pertinent to infrared observations, including sky emission and instrumental background subtraction, flat-fielding, bad pixels correction. It should be noted that the accuracy to which the sky and instrument contributions are removed may be critical when looking for very faint and extended structures such as circumstellar disks or envelopes.

Each resulting image can then be described as the sum of the residual contributions from the occulted star (scattered light, speckle noise corresponding to high order turbulence modes, etc.) and the potential circumstellar emission that we wish to detect. The next step therefore consists in removing, as thoroughly as possible, the residual contributions from the occulted star by subtracting the image of the comparison star, after proper re-centering and scaling. The re-centering is usually needed to compensate for mechanical flexure between the observations of the target and the comparison star and for uncertainties in the centering of both objects behind the mask during the observations. Typical accuracies for the re-centering are of the order of 0.1 to 0.2 pixel. The scaling factor is determined by dividing the image of the target by the image of the comparison star. More details on the reduction procedure can be found in Mouillet et al. (1997a).

5 Astrophysical results

Astrophysical results have been obtained on various programmes, either with the ADONIS coronograph or with the Observatoire de Grenoble visitor instrument.

5.1 Circumstellar disks

Circumstellar disks around Main Sequence stars are now known to exist, as revealed by IRAS measurements of infrared excesses, and in the case of β Pictoris, as shown by direct coronographic images of the light scattered by the dust (Smith & Terrile 1984). Such disks are important since they provide clues on the formation and evolution of planetary systems. Whereas classical observations of β Pictoris enabled to observe its circumstellar disk down to typically 80 AU from the star, ADONIS coronographic observations (Mouillet et al. 1997a), as well as HST observations (Burrows, Krist, & Stapelfeldt 1995), allowed to detect it down to about 20 AU, ie. inside the planet orbits in our Solar System, and find indirect informations on the presence of planets (Mouillet et al. 1997b).

Fig. 6 illustrates the ADONIS coronographic observations of the β Pictoris circumstellar disk in scattered light at 1.25 μm. The disk is detected down to 24 AU and a warp is clearly seen in the inner part of the disk (Mouillet et al. 1997a).

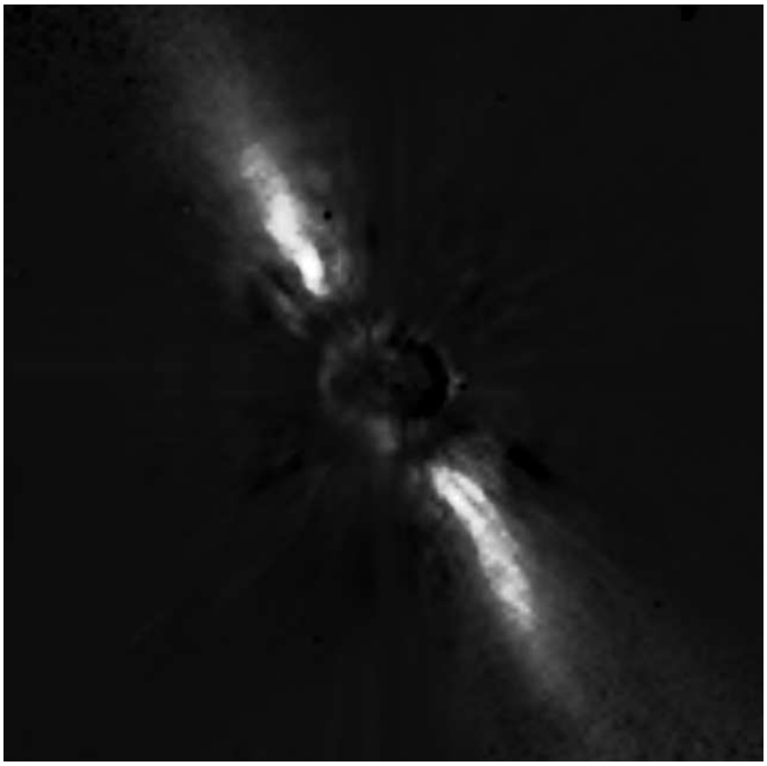

Figure 6: The β Pictoris disk observed with the ADONIS coronograph at 1.25 μm.

5.2 Brown dwarfs

The first brown dwarfs associated to nearby stars have been discovered in coronographic, tip-tilt corrected, visible images (Nakajima et al. 1995; Golimowski et al. 1995). The high luminosity contrast between the brown dwarf and its parent star indeed requires coronographic observations to block out the light of the star. The temperature of brown dwarfs ($\sim$ 2000 K) also suggests that the best wavelength range to observe them is the near infrared. Several surveys to detect other brown dwarfs are underway on 4 meter telescopes equipped with adaptive optics systems. In particular, a systematic search for brown dwarfs around nearby southern M dwarfs has been undertaken with the ADONIS coronograph (Beuzit et al. 1998). During the 7 nights of observation already devoted to that survey, 9 faint objects have been detected, with $\Delta\ m_K$ ranging from 5 to more than 10 at distances greater than 2$''$ from the primary. Follow-up observations are of course required to determine if the detected objects are physical companions (low mass stars or brown dwarfs) or background stars. As of September 1998, complementary observations, obtained about 1 year after the detections, have allowed to identify 5 of the 9 sources as background stars. Fig. 7 illustrates the detection in March 98 of a faint source (Δ K = 7) located 6.7$''$ away from a M1 dwarf.

5.3 η Carinae

η Carinae is an evolved super massive star, classified as an extreme Luminous Blue Variable star. The star has expelled its upper layers in a great eruption in the 19th century and is now surrounded by a 12$''$ $\times$ 18$''$ nebula composed of dust and gas, mainly emitting in scattered light from the central source. The stellar core of η Carinae has a K magnitude of 0.8 and the britghness contrast with the surrounding nebulae is $\approx$ 12 mag.arcsec^{-2}. Adaptive optics observations of this object do not allow to image the surrounding nebulae (individual integration time with a spectral resolution of 2000 is $<$ 200 ms). In order to detect the nebula, and get the highest signal to noise ratio over its extension, we observed this object in coronographic mode with a 4$''$ diameter occulting mask in the helium line (2.0581 μm). The resulting image at 0.2$''$ spatial resolution is shown by Le Mignant et al. (1998), in these proceedings.

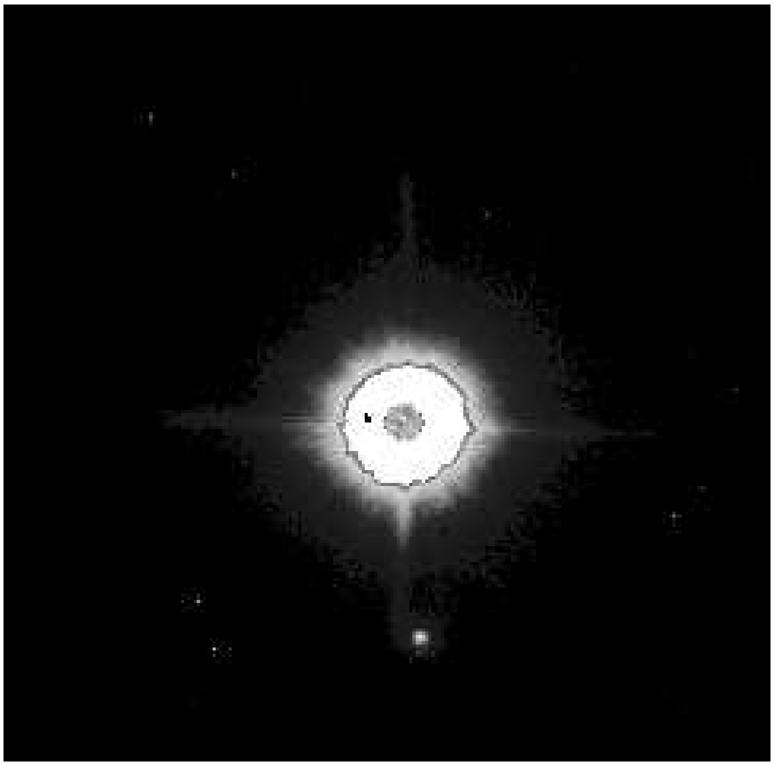

Figure 7: Detection of a faint source around a nearby M dwarf with the ADONIS coronograph.

6 Coronography on very large telescopes

The new generation of very large telescopes will be equipped with adaptive optics coronographs (VLT, Gemini, Subaru, etc.) and will dedicate a significant fraction of their observing time to astrophysical programmes such as the searches for very low mass stars, brown dwarfs, extra-solar planets and circumstellar disks (Morris et al. 1996; Lagrange et al. 1997).

As part of the preparation of the Scientific Analysis Report for the VLT Nasmyth Adaptive Optics System (NAOS), we have simulated observations of β Pictoris-like disks at 2.2 μm, with NAOS and its associated infrared camera CONICA (Lagrange et al. 1998). A 1 AU gap due to planet perturbation at 20 AU from the star would be detected with a $0.3''$ mask (Fig. 8). The Strehl ratio is 0.7 for the simulated image.

7 Acknowledgments

We are grateful to all colleagues who helped with the development of the ADONIS coronographic mode, especially P. Puget, E. Stadler and Y. Magnard at Observatoire de Grenoble for designing and manufacturing the focal plane unit and the mask suspension system, J. Seerveld at CFHT for cutting the occulting masks, and F. Lacombe at Observatoire de Paris for adding to the camera acquisition software the functions needed to control the occulting mask positioning. We also wish to thank D. Bonaccini, N. Hubin, P. Léna and F. Malbet for helpful discussions. Additional thanks are extended to the ADONIS team as well as the ESO La Silla staff for their active help during the integration and tests of the coronograph on the 3.6 meter telescope. The development of the ADONIS coronograph was carried out under ESO contract No 46578/INS/96/6157/GWI.

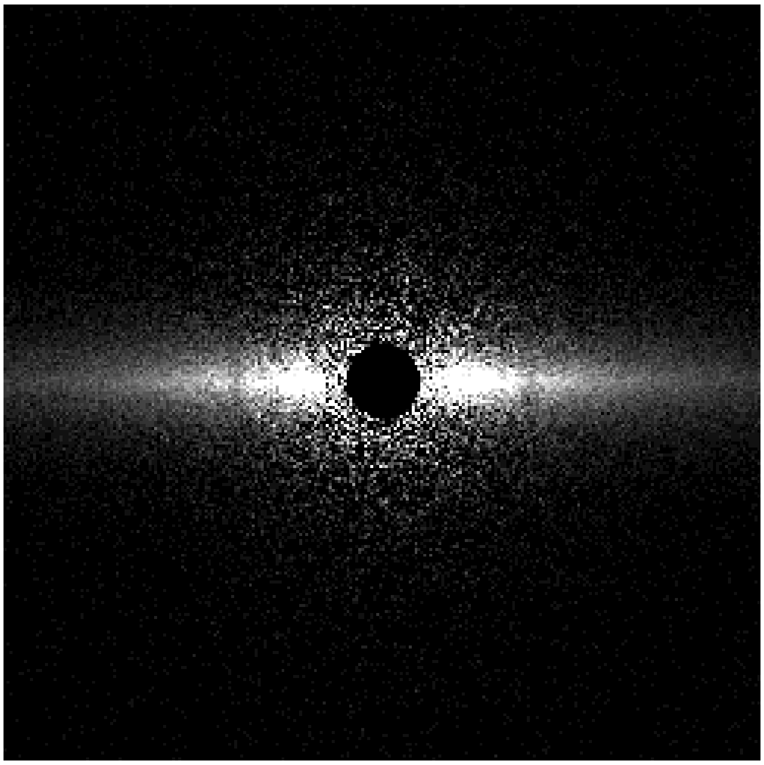

Figure 8: Simulation of a β Pictoris-like disk observed with NAOS and CONICA.

References

Beuzit, J.-L., Delfosse, X., Forveille, T., Udry, S., Mayor, M., Perrier, C., Mariotti, J.-M., & Segransan, D. 1998, in Astronomy with Adaptive Optics (these proceedings), ed. D. Bonaccini

Beuzit, J.-L., et al. 1997a, Exp. Astron., 7, 285

Beuzit, J.-L., Lacombe, F., Mariotti, J.-M., Perrier, C., & Rouan, D. 1990, in Astrophysics with Infrared Arrays, ed. R. Elston, Vol. 14 (ASP Conference Series), 316

Beuzit, J.-L., Mouillet, D., Lagrange, A.-M., & Paufique, J. 1997b, A&AS, 125, 175

Burrows, C., Krist, J., & Stapelfeldt, K. 1995, BAAS, 187, 3205

Clampin, M., Paresce, F., & Roberto, M. 1994, in Instrumentation in Astronomy VIII, ed. D. Craword & E. Craine, Vol. 2198, 172

Golimowski, D., Nakajima, T., Kulkarni, S., & Oppenheimer, B. 1995, ApJ, 444, L101

Golimowski, D. A., Durrance, S. T., & Clampin, M. 1993, ApJ, 411, L41

Lagrange, A.-M., et al. 1997, VLT Nasmyth Adaptive Optics System - Scientific Analysis Report, Technical Report VLT-TRE-NAO-11650-9000, ESO

Lagrange, A.-M., et al. 1998, in Adaptive Optical System Technologies, ed. D. Bonaccini & R. K. Tyson, Vol. 3353, 591

Le Mignant, D., et al. 1998, in Astronomy with Adaptive Optics (these proceedings), ed. D. Bonaccini

Lowrance, P., et al. 1998, in NICMOS and the VLT, ed. W. Freudling & R. Hook, Vol. 55, 96

Malbet, F. 1996, A&AS, 115, 161

Morris, S., Davidge, T., Hutchings, J., Stetson, P., Durand, D., Crabtree, D., & Cote, P. 1996, Science drivers for adaptive optics on gemini north, Technical report, NRC-CNRC

Mouillet, D., Lagrange, A.-M., Beuzit, J.-L., & Renaud, N. 1997a, A&A, 324, 1083

Mouillet, D., Larwood, J., Papaloizou, J., & Lagrange, A.-M. 1997b, MNRAS, 292, 896

Nakajima, T., Oppenheimer, B., Kulkarni, S., Golimowski, D., Matthews, K., & Durrance, S. 1995, Nature, 378, 463

Seerveld, J. 1998, in Optical Astronomical Instrumentation, ed. S. D'Odorico, Vol. 3355, 987

Smith, B., & Terrile, R. 1984, Science, 226, 1421

Watson, S. M., Mills, J. P., Gaiser, S. L., & Diner, D. J. 1991, Appl. Opt., 30, 22